

Synthesizing 4D Magnetic Resonance Angiography From 3D Time-of-Flight Using Deep Learning: A Feasibility Study

Review began 04/25/2024

Review ended 05/15/2024

Published 05/21/2024

© Copyright 2024

Wada et al. This is an open access article distributed under the terms of the Creative Commons Attribution License CC-BY 4.0., which permits unrestricted use, distribution, and reproduction in any medium, provided the original author and source are credited.

Akihiko Wada ¹, Toshiya Akatsu ², Yutaka Ikenouchi ¹, Michimasa Suzuki ³, Toshiaki Akashi ¹, Akifumi Hagiwara ¹, Mitsuo Nishizawa ¹, Katsuhiro Sano ¹, Koji Kamagata ¹, Shigeki Aoki ¹

1. Department of Radiology, Juntendo University School of Medicine, Tokyo, JPN 2. Department of Radiology, Juntendo University Hospital, Tokyo, JPN 3. Department of Radiology, Juntendo University Urayasu Hospital, Chiba, JPN

Corresponding author: Akihiko Wada, a-wada@juntendo.ac.jp

Abstract

Objective and background

This study aimed to develop a deep convolutional neural network (DCNN) model capable of generating synthetic 4D magnetic resonance angiography (MRA) from 3D time-of-flight (TOF) images, allowing estimation of temporal changes in arterial flow. TOF MRA provides static information about arterial structures through maximum intensity projection (MIP) processing, but it does not capture the dynamic information of contrast agent circulation, which is lost during MIP processing. Considering the principles of TOF, it is hypothesized that dynamic information about arterial blood flow is latent within TOF signals. Although arterial spin labeling (ASL) can extract dynamic arterial information, ASL MRA has drawbacks, such as longer imaging times and lower spatial resolution than TOF MRA. This study's primary aim is to extend the utility of TOF MRA by training a machine-learning model on paired TOF and ASL data to extract latent dynamic information from TOF signals.

Methods

A DCNN combining a modified U-Net and a long-short-term memory (LSTM) network was trained on a dataset of 13 subjects (11 men and two women, aged 42-77 years) using paired 3D TOF MRA and 4D ASL MRA images. Subjects had no history of cerebral vessel occlusion or significant stenosis. The dataset was acquired using a 3T MRI system with a 32-channel head coil. Preprocessing involved resampling and intensity normalization of TOF and ASL images, followed by data augmentation and arterial mask generation. The model learned to extract flow information from TOF images and generate 8-phase 4D MRA images. The precision of flow estimation was evaluated using the coefficient of determination (R^2) and Bland-Altman analysis. A board-certified neuroradiologist validated the quality of the images and the absence of significant stenosis in the major cerebral arteries.

Results

The generated 4D MRA images closely resembled the ground-truth ASL MRA data, with R^2 values of 0.92, 0.85, and 0.84 for the internal carotid artery (ICA), proximal middle cerebral artery (MCA), and distal MCA, respectively. Bland-Altman analysis revealed a systematic error of -0.06, with 95% agreement limits ranging from -0.18 to 0.12. Additionally, the model successfully identified flow abnormalities in a subject with left MCA stenosis, displaying a delayed peak and subsequent flattening distal to the stenosis, indicative of reduced blood flow. Visualization of the predicted arterial flow overlaid on the original TOF MRA images highlighted the spatial progression and dynamics of the flow.

Conclusions

The DCNN model effectively generated synthetic 4D MRA images from TOF images, demonstrating its potential to estimate temporal changes in arterial flow accurately. This non-invasive technique offers a promising alternative to conventional methods for visualizing and evaluating healthy and pathological flow dynamics. It has significant potential to improve the diagnosis and treatment of cerebrovascular diseases by providing detailed temporal flow information without the need for contrast agents or invasive procedures. The practical implementation of this model could enable the extraction of dynamic cerebral blood flow information from routine brain MRI examinations, contributing to the early diagnosis and management of cerebrovascular disorders.

Categories: Neurology, Neurosurgery, Radiology

Keywords: neuro mri, u-net, lstm networks, deep convolutional network, deep neural network, asl mra, tof mra

Introduction

Time-of-flight (TOF) magnetic resonance angiography (MRA) has long been a cornerstone in vascular imaging, playing a crucial role in the diagnosis of cerebrovascular disorders and cerebral aneurysms since the early days of clinical MRI [1-6]. Despite emerging advanced technologies, 3D TOF-MRA remains a mainstay for non-contrast vascular imaging in central and peripheral regions due to its ability to provide

How to cite this article

Wada A, Akatsu T, Ikenouchi Y, et al. (May 21, 2024) Synthesizing 4D Magnetic Resonance Angiography From 3D Time-of-Flight Using Deep Learning: A Feasibility Study. Cureus 16(5): e60803. DOI 10.7759/cureus.60803

high spatial resolution images of cerebral arteries (6). This resolution comes from the "inflow effect," one of the three flow-related MR phenomena, in which "fresh" blood entering the imaging slice appears with a high signal [4,7].

Arterial spin labeling (ASL)-MRA, a recent advancement in magnetic resonance angiography, utilizes arterial blood labeled with RF pulses as an endogenous tracer, such as TOF, to represent arterial flow [7-11]. This technique uses short TE settings, which have been reported to mitigate the loss of flow-related signal from laminar and turbulent flows and susceptibility artifacts from metallic devices, thereby improving image quality [12-18].

Furthermore, ASL-MRA allows dynamic signal collection with appropriate timing delays after labeling to achieve 4D MRA with temporal information, which is not possible with TOF and was previously only possible with conventional angiography [14,19-25].

However, when comparing the imaging conditions of ASL-MRA and 3D TOF MRA, it is noteworthy that while ASL-MRA provides temporal information, it does so at the cost of lower spatial resolution and longer imaging times, which are significant disadvantages compared to TOF MRA [18,23].

Although both ASL-MRA and TOF-MRA rely on contrasting arterial flow against the background, the longer signal acquisition time of TOF-MRA, ten times that of ASL in our setting, suggests that it may inherently capture more comprehensive flow information. However, this information is underutilized in conventional 3D TOF-MRA with maximum intensity projection.

Therefore, this study aims to leverage the rich flow information within TOF data using machine learning to extract temporal flow dynamics and generate 4D MRA. Our objective is to develop a method that can accurately estimate changes in arterial flow over time, potentially offering a noninvasive and efficient alternative to existing techniques for healthy subjects and those with pathological flow conditions.

Materials And Methods

Study design

This study aims to generate 4D MRA using machine learning by estimating temporal changes in arterial flow from 3D TOF MRA images. The institutional ethics committee approved the retrospective study with an opt-out option for informed consent.

Data acquisition

All data was collected using a 3T MRI system (Vantage Centurian, Canon Medical Systems) equipped with a 32-channel head coil. The dataset consisted of paired 3D TOF MRA and 4D ASL MRA images from 13 subjects (11 men and 2 women) aged between 42 and 77 years with no history of cerebral vessel occlusion or significant stenosis (Table 1). The imaging parameters for the 3D TOF MRA and 4D ASL MRA are described in Table 2. A board-certified neuroradiologist with more than 28 years of experience confirmed the image quality, the absence of significant stenosis (>50%) in the major cerebral arteries, and flow differences between hemispheres.

Parameter	Description
Imaging Modalities	Paired 3D Time-of-Flight (TOF) magnetic resonance angiography (MRA) and 4D Arterial Spin Labeling (ASL) MRA
Number of Subjects	13 subjects
Gender Distribution	11 men, 2 women
Age Range	42 to 77 years
Clinical Background	No history of cerebral vessel occlusion or significant stenosis

TABLE 1: Dataset Characteristics

Parameter	3D TOF MRA	4D ASL MRA
FOV	224mm	200mm
Matrix	224x448	224x224
Slices	152 (1mm thick)	200
TR/TE	18/3.9 msec	3.7/0.1 msec
Flip Angle	15°	6°
Scan Time	2 min 56 sec	11 min 42 sec
Phases	-	8 (150-1550 msec)
Final Voxel Size	512x512x152	256x256x200

TABLE 2: Imaging Parameters of 3D TOF MRA and 4D ASL MRA

FOV: Field of View, MRA: Magnetic Resonance Angiography, TOF: Time-of-Flight, ASL: Arterial Spin Labeling, TR: Repetition Time, TE: Echo Time

Pre-processing

Both 3D TOF and 8-phase ASL MRA images were acquired in DICOM (Digital Imaging and Communications in Medicine) format. The OsiriX DICOM Viewer (Pixmeo SARL, Geneva, Switzerland) was used to resample the 8-phase ASL flow images to match the TOF image positions [26]. The resampled ASL images were exported as 16-bit TIFF images with a window width of 2000 and a window center of 1000, then converted to 8-bit grayscale PNG format and resized to 128x128 pixels using interpolation to reduce data size. The TOF images underwent the same conversion process using the default display settings.

Arterial masks were generated for the TOF and ASL images to focus the model on relevant areas and reduce background noise. Intensity values of the 8-bit grayscale images (0-255) were normalized to the 0-1 range. A 3D binary mask was created by identifying regions within the 8phase ASL images where the difference between the maximum and minimum intensity values exceeded 0.25, representing arterial vessels. Then, this mask was applied to the original ASL images for training.

Data splitting and model validation

The dataset was divided into training and testing sets. Thirteen subjects with various conditions were used for training, while one healthy subject and one post-aneurysm treatment patient were reserved for testing. This ensured an unbiased evaluation of the model's performance. The training set was used to train the model, while the testing set was used to assess its effectiveness in generating 4D MRA images using performance metrics such as accuracy and loss.

Machine learning models

Deep convolutional neural networks (DCNNs) were developed using the Neural Network Console, an open-source Python library (version 3.6.2) provided by Sony Network Communications Inc (Tokyo, Japan) [27].

Two learning processes were implemented:

Modified U-Net

This model was trained to estimate eight-phase flow changes from a single TOF image. It consists of a convolutional layer followed by down-sampling and up-sampling layers, ultimately generating eight normalized flow images [28,29].

Long-Short-Term Memory (LSTM)

To ensure spatial consistency of flow estimation along the z-axis (proximal to distal), the modified Unet was integrated into an LSTM network [30]. This recurrent neural network architecture, specifically designed for time-series data, uses the modified U-Net as its memory cell. It employs four-layer convolutional neural networks for the forget input and output gates. By processing 152 consecutive axial images, the LSTM maintains long-term memory along the z-axis, preserving the estimated flow's spatial consistency in axial and planar dimensions.

The architecture of the combined model is illustrated in Figure 1 and is further detailed in the supplementary materials.

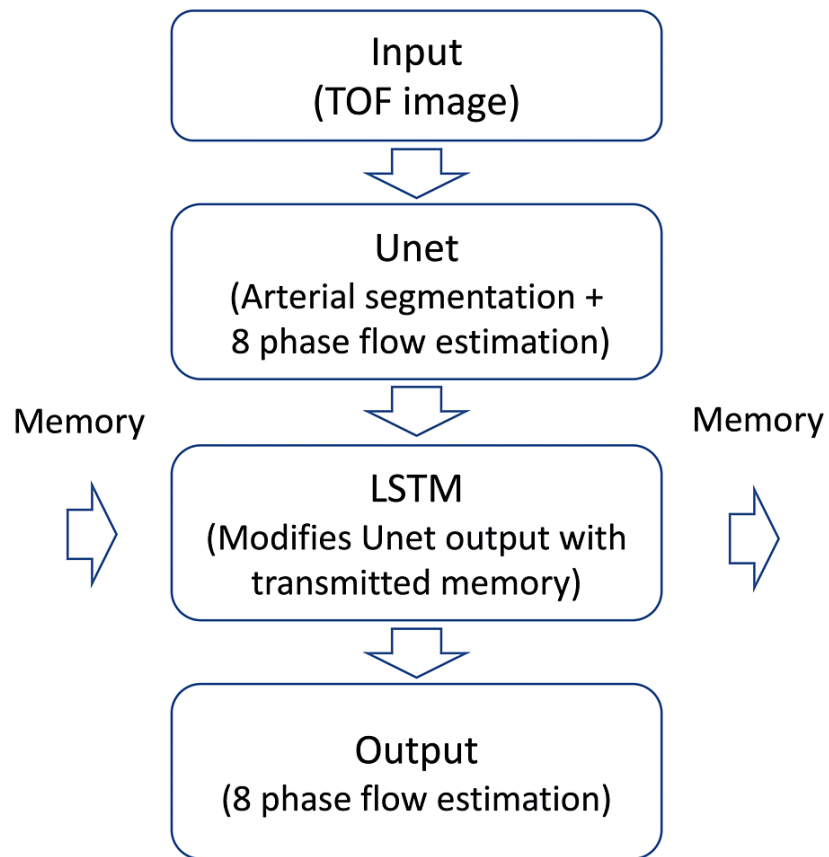


FIGURE 1: Structure of the machine learning model synthetic 8-phase flow from the TOF signal

The modified Unet extracts arterial regions from the time-of-flight (TOF) image and converts the intravascular signal into an 8-phase flow. The long-short-term memory (LSTM) model was used to maintain the spatial consistency between the transformation from TOF to eight-phase flow images and the direction of arterial flow in the brain. The detailed structure of these models can be seen in the Appendices.

Training

The model used the mean squared error as the loss function, measuring the pixel-level discrepancy between the predicted and ground-truth normalized eight-phase ASL flow signals. Training parameters included a maximum of 1000 epochs, an optimization algorithm of Adam with an initial learning rate of 0.001, α and β values of 0.001 and 0.9 respectively, and a learning rate scheduler of cosine annealing.

Evaluation

Two metrics were used to evaluate the model's performance: the coefficient of determination (R^2), which assesses the goodness of fit between the predicted 8-phase flow and the actual ASL flow signal, and Bland-Altman analysis, which evaluates the agreement between the predicted and actual flow by calculating the systematic error (mean difference), precision (standard deviation), and 95% agreement limits. The regions of interest were manually placed in the internal carotid artery and the proximal and distal middle cerebral arteries to analyze the relationship between predicted and actual flow signals.

Results

The DCNN model successfully generated 8-phase 4D MRA images that resemble the reference ASL MRA data (Figure 2). In a healthy test subject, the R^2 values for flow estimation were 0.92, 0.85, and 0.84 for the internal carotid artery, the proximal middle cerebral artery (MCA) and the distal MCA, respectively (Figure 3). These findings were statistically significant ($p < 0.001$). Bland-Altman analysis showed a systematic error of -0.06 with 95% agreement limits ranging from -0.18 to 0.12 (Figure 4).

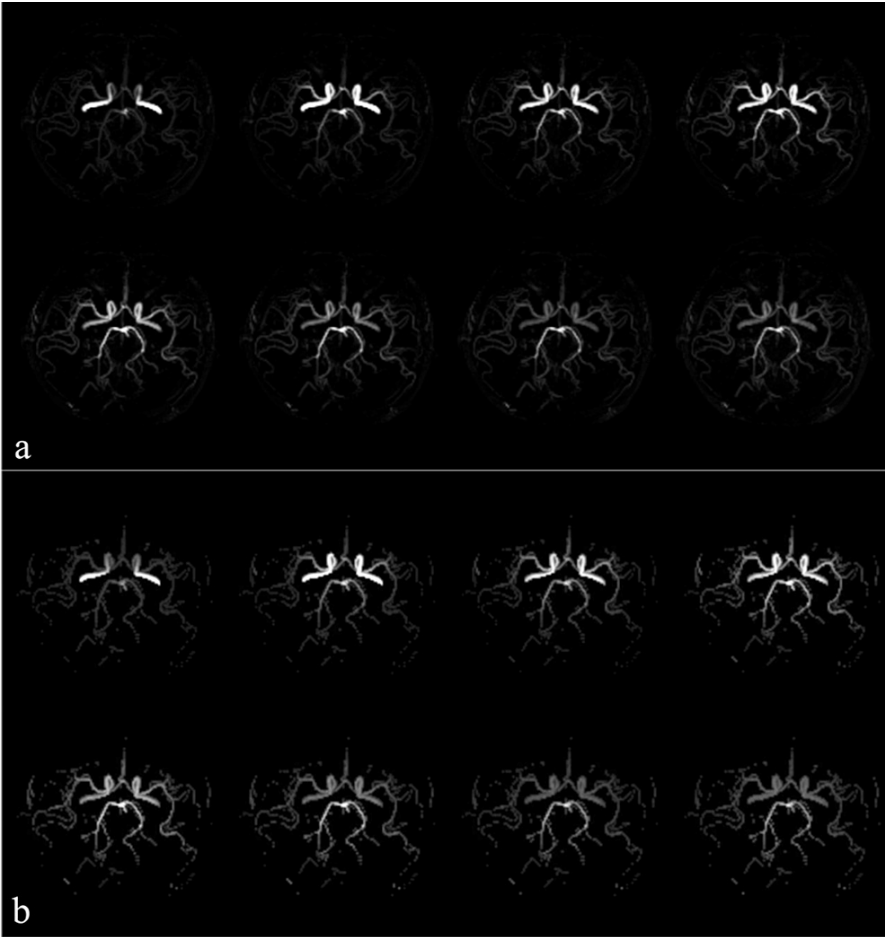


FIGURE 2: Comparison of synthetic and ground-truth 4D MRA.

(a) Synthetic 8-phase 4D magnetic resonance angiography (MRA) generated from time-of-flight (TOF) data using the deep convolutional neural network (DCNN) model. (b) 4D ground truth MRA acquired by arterial spin labeling (ASL). Both images are shown in the same axial projection.

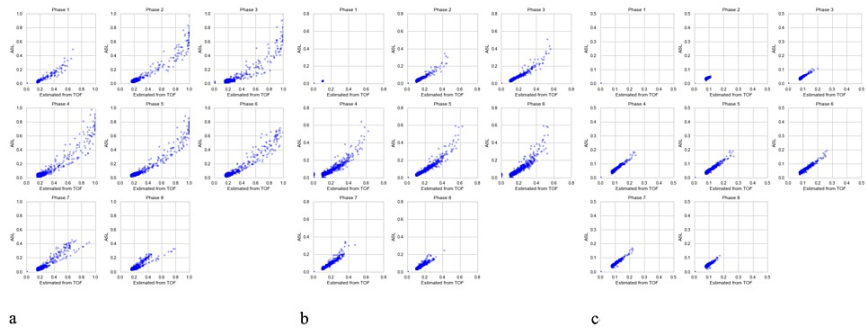


FIGURE 3: Scatter plots comparing the estimated 8-phase flow from TOF with the actual ASL flow in a healthy test subject.

(a) Internal carotid artery (ICA). (b) Proximal middle cerebral artery (MCA). (c) Distal MCA. The x-axis represents the estimated flow from time-of-flight (TOF), and the y-axis represents the corresponding arterial spin labeling (ASL) signal value, with both scales normalized between 0 and 1.

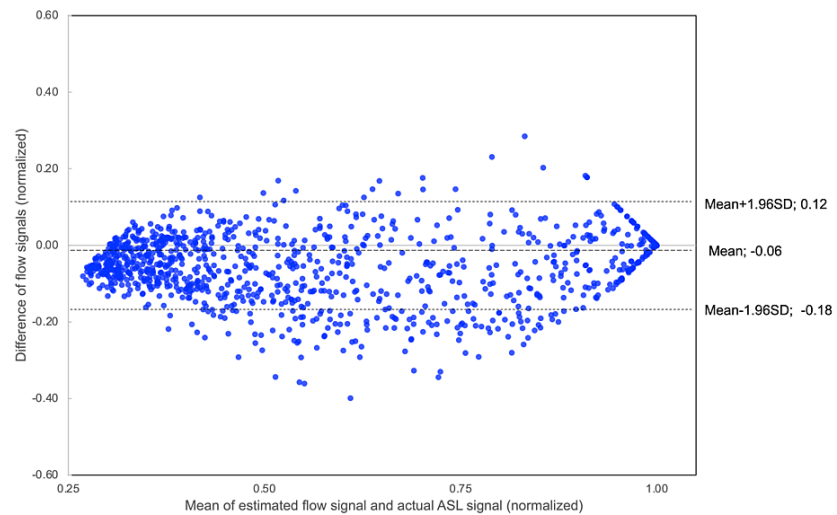


FIGURE 4: Bland-Altman graph comparing estimated 8-phase flow with actual arterial spin labeling (ASL) flow in the internal carotid artery.

The x-axis represents the mean difference between the two signals, and the y-axis represents the mean of the two signals. The systematic error (mean difference) is -0.06, and the 95% limits of agreement are 0.12 and -0.18, indicating good agreement between the estimated and actual flow signals.

Overlaying the predicted arterial flow (in red) on the original 3D TOF MRA image visualizes the flow's reach throughout the vasculature (Figure 5). In a test subject with left MCA stenosis, the 8-phase flow signal generated exhibited a delayed peak and subsequent flattening distal to the stenosis, indicating reduced flow (Figure 6).

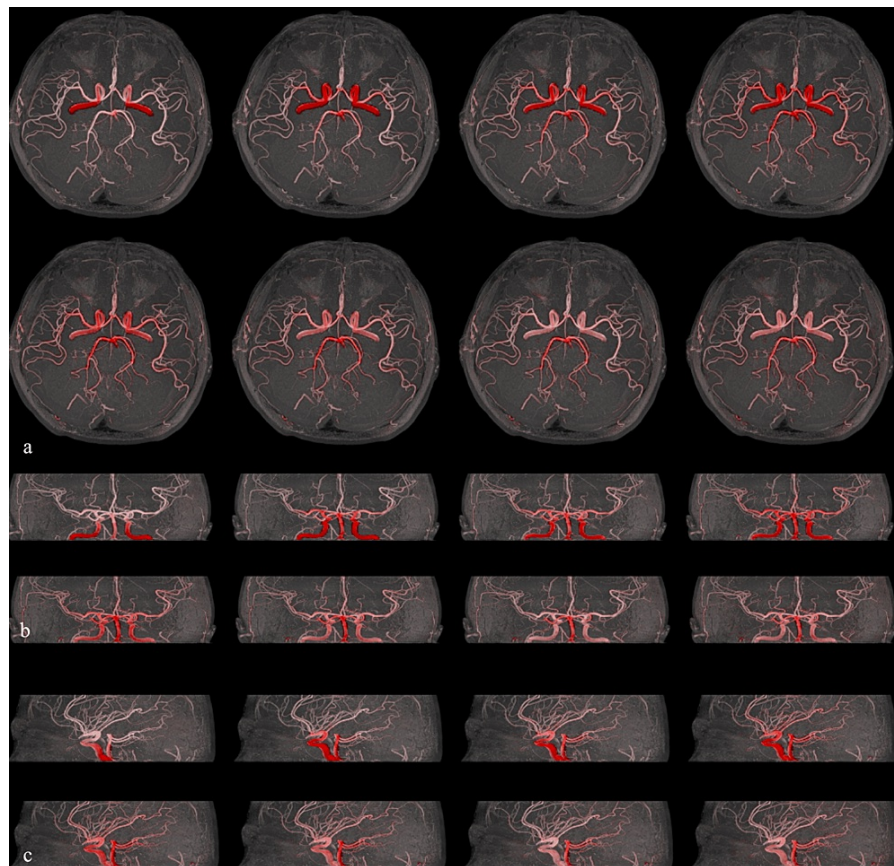


FIGURE 5: Visualization of synthetic 8-phase flow progression overlaid on the original 3D TOF MRA.

The estimated flow is depicted in red, and the original time-of-flight (TOF) magnetic resonance angiography (MRA) is superimposed in white. (a) Axial projection. (b) Lateral projection. This visualization allows for the observation of vascular structures and the progression of arterial flow over time.

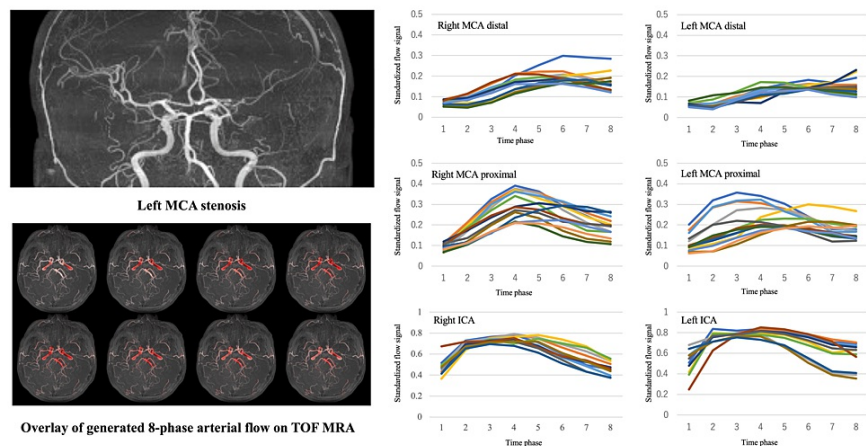


FIGURE 6: Synthetic 4D MRA in a left middle cerebral artery stenosis case.

The top left is a frontal view of time-of-flight (TOF) magnetic resonance angiography (MRA), and the bottom left is an overlay of the generated 8-phase arterial signal to TOF MRA. On the right are the time signal changes of the generated 8-phase flow signals of the left and right internal carotid arteries (ICAs) and the proximal and distal middle cerebral arteries (MCAs). Generated time signal curve showing a delayed peak distal to the stenosis and subsequent flattening, indicating reduced blood flow.

Discussion

This study demonstrates the feasibility of using a DCNN model to generate synthetic 4D MRA from 3D TOF images. The model effectively estimated temporal changes in arterial flow in healthy subjects, achieving high R^2 values and good agreement with ground-truth ASL MRA data. Furthermore, visualization of flow progression and identification of flow abnormalities in a stenosis case highlight the potential of this technique for clinical applications.

Applications and unmet needs of current TOF MRA

TOF-MRA provides static information about the structure of arteries through MIP processing, similar to traditional cerebral angiography. However, it does not provide dynamic information about the contrast agent's circulation dynamics, as this information is lost during MIP processing. Considering the principles of TOF, it can be hypothesized that dynamic information about arterial blood flow is also latent within TOF signals.

ASL is a technique that can extract dynamic information from arteries, but compared to TOF-MRA, ASL-MRA has the disadvantages of longer imaging times and lower spatial resolution. The main aim of this study is to extend the utility of TOF-MRA by using a machine learning model trained on paired TOF and ASL data to extract the latent dynamic information from TOF signals.

In general, brain MRI examinations use TOF signals to indicate the static information of arteries, showing their shape. This has proven effective in detecting aneurysms and vascular stenosis. Given the principles of TOF signals, it can be inferred that dynamic information about arteries is also latent.

Expected clinical impact of 4D MRA

This proposed method offers several practical applications that could benefit general clinical practice:

Extending the Utility of TOF MRA: The proposed method enhances the capabilities of TOF MRA beyond its traditional use by extracting dynamic flow information from TOF signals.

Utilizing Dynamic Information: The dynamic information lost during MIP processing can provide a more comprehensive view of arterial flow.

Screening for Cerebrovascular Disorders: During routine screenings, the proposed method could detect minor blood flow reductions from time-series blood flow changes estimated from TOF, potentially predicting the risk of cerebrovascular disorders.

Comparison of TOF and ASL techniques

TOF and ASL MRA exploit the contrast between flowing blood and static tissue to visualize vascular structures. However, they differ in their signal acquisition time and the type of information they provide. ASL, with its rapid filling of the k-space and short echo time, achieves a temporal resolution of 200 milliseconds, enabling the acquisition of multiple 3D images within a short timeframe. In contrast, TOF MRA has a longer acquisition time, approximately ten times longer than ASL in our study. This difference inspired the current research, as the longer acquisition time of TOF may inherently capture more comprehensive flow information compared to the snapshot-like nature of ASL.

Model architecture and rationale

The combination of U-Net and LSTM networks was chosen for this study due to their complementary strengths. The U-Net architecture excels at image segmentation and transformation tasks, allowing for the extraction of arterial regions from TOF images and estimating eight-phase flow changes. The LSTM network, with its ability to retain long-term memory, ensures spatial consistency of flow estimation along the z-axis, providing a more accurate representation of the flow dynamics within the vasculature.

Limitations

This preliminary study has several limitations. To achieve feasible training times, the spatial resolution of the output images was reduced compared to the original TOF MRA. Furthermore, the training dataset was limited in size and lacked sufficient pathological flow data. The preprocessing steps involved converting DICOM data to lower-quality formats and using interpolation, which may have resulted in some loss of the original MR signal information. Although these steps were necessary due to current limitations in data handling capacity, they may affect the authenticity of the images. Future studies should incorporate larger and more diverse datasets, including various pathologies, to further validate and improve the generalizability of the model. Additionally, as processing environments advance, it will be possible to handle higher-quality data, thereby reducing the need for such preprocessing steps and preserving the integrity of the original MR signals.

Future directions

Future research can be extended in several ways. Improving the spatial resolution may involve exploring

alternative network architectures or employing data-augmentation techniques, which could enable the generation of high-resolution 4D MRA while maintaining efficient training times. Expanding the training dataset to include a wider range of pathologies and flow conditions will enhance the model's generalizability and robustness. Additionally, implementing methods to quantify the uncertainty associated with the model's predictions can improve its reliability for clinical decision-making. Finally, investigating techniques to understand how the model arrives at its predictions will increase trust and acceptance in clinical settings.

Conclusions

This study demonstrates the potential of deep learning techniques to extract temporal flow information from TOF MRA and generate synthetic 4D MRA. The proposed method offers a promising noninvasive approach to visualizing and evaluating arterial flow dynamics, which may aid in the diagnosis and management of cerebrovascular diseases.

Appendices

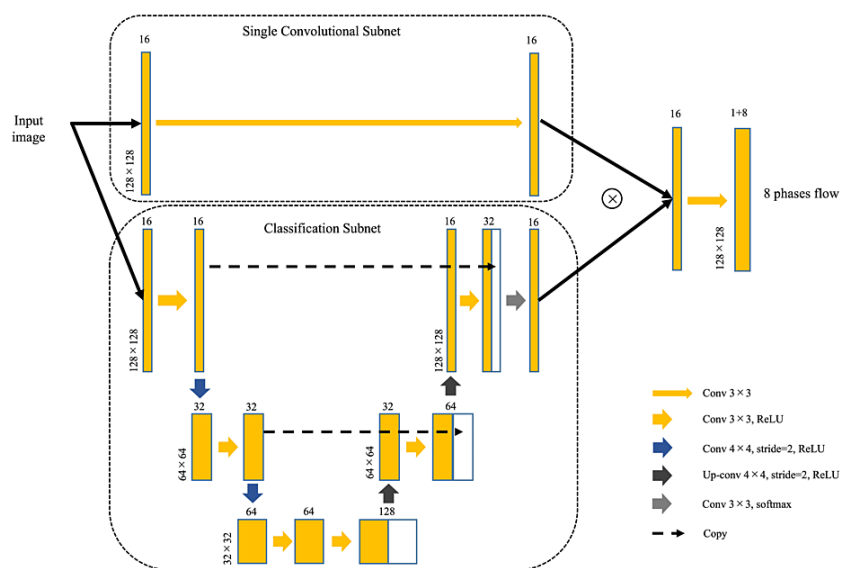


FIGURE 7: Detailed architecture of the modified Unet network used to estimate the 8-phase flow from the time-of-flight (TOF) signal.

The network uses a combination of convolutional layers and rectified linear units (ReLU) to extract features and generate flow estimations.

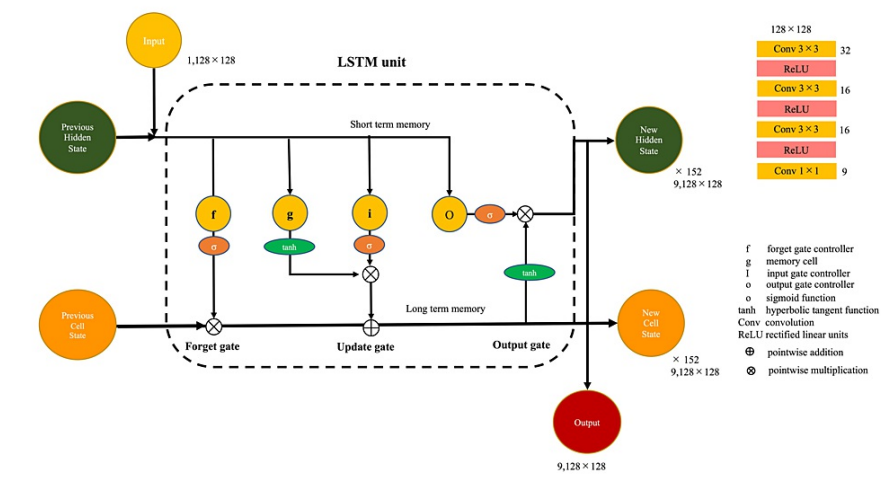


FIGURE 8: Detailed architecture of the long-short-term memory (LSTM) network used to maintain spatial consistency of flow estimation along the z-axis.

The LSTM employs memory cells and gate controllers to regulate the information flow and preserve temporal relationships within the generated 4D magnetic resonance angiography (MRA).

Additional Information

Author Contributions

All authors have reviewed the final version to be published and agreed to be accountable for all aspects of the work.

Concept and design: Akihiko Wada, Toshiya Akatsu

Drafting of the manuscript: Akihiko Wada, Toshiya Akatsu, Yutaka Ikenouchi

Acquisition, analysis, or interpretation of data: Toshiya Akatsu, Yutaka Ikenouchi, Michimasa Suzuki, Toshiaki Akashi, Akifumi Hagiwara, Mitsuo Nishizawa, Katsuhiko Sano, Koji Kamagata, Shigeki Aoki

Critical review of the manuscript for important intellectual content: Michimasa Suzuki, Toshiaki Akashi, Akifumi Hagiwara, Mitsuo Nishizawa, Katsuhiko Sano, Koji Kamagata, Shigeki Aoki

Supervision: Michimasa Suzuki, Toshiaki Akashi, Shigeki Aoki

Disclosures

Human subjects: Consent was obtained or waived by all participants in this study. Juntendo University Clinical Research Review Committee issued approval M21-0011. **Animal subjects:** All authors have confirmed that this study did not involve animal subjects or tissue. **Conflicts of interest:** In compliance with the ICMJE uniform disclosure form, all authors declare the following: **Payment/services info:** All authors have declared that no financial support was received from any organization for the submitted work. **Financial relationships:** All authors have declared that they have no financial relationships at present or within the previous three years with any organizations that might have an interest in the submitted work. **Other relationships:** All authors have declared that there are no other relationships or activities that could appear to have influenced the submitted work.

Acknowledgements

The authors would like to express their gratitude to the Japan Society for the Promotion of Science (JSPS) for their financial support through the JSPS KAKENHI Grant Number JP22K07674.

References

1. Axel L: Blood flow effects in magnetic resonance imaging. *AJR Am J Roentgenol*. 1984, 143:1157-66. [10.2214/ajr.143.6.1157](https://doi.org/10.2214/ajr.143.6.1157)
2. Bradley WG Jr, Waluch V: Blood flow: magnetic resonance imaging. *Radiology*. 1985, 154:443-50. [10.1148/radiology.154.2.3966131](https://doi.org/10.1148/radiology.154.2.3966131)
3. Axel L, Shimakawa A, MacFall J: A time-of-flight method of measuring flow velocity by magnetic resonance

- imaging. *Magn Reson Imaging*. 1986, 4:199-205. [10.1016/0730-725x\(86\)91059-3](#)
4. Guit GL, Bluemm R, Rohmer J, Wenink AC, Chin JG, Doornbos J, van Voorthuisen AE: Levotransposition of the aorta: identification of segmental cardiac anatomy using MR imaging. *Radiology*. 1986, 161:673-9. [10.1148/radiology.161.3.3786718](#)
5. Frahm J, Bruhn H, Gyngell ML, Merboldt KD, Hänicke W, Sauter R: Localized proton NMR spectroscopy in different regions of the human brain in vivo. Relaxation times and concentrations of cerebral metabolites. *Magn Reson Med*. 1989, 11:47-63. [10.1002/mrm.1910110105](#)
6. Wehrli FW: Time-of-flight effects in MR imaging of flow. *Magn Reson Med*. 1990, 14:187-93. [10.1002/mrm.1910140205](#)
7. Edelman RR, Siewert B, Adamis M, Gaa J, Laub G, Wielopolski P: Signal targeting with alternating radiofrequency (STAR) sequences: application to MR angiography. *Magn Reson Med*. 1994, 31:233-8. [10.1002/mrm.1910310219](#)
8. Edalati M, Hastings MK, Muccigrosso D, et al.: Intravenous contrast-free standardized exercise perfusion imaging in diabetic feet with ulcers. *J Magn Reson Imaging*. 2019, 50:474-80. [10.1002/jmri.26570](#)
9. Buxton RB, Frank LR, Wong EC, Siewert B, Warach S, Edelman RR: A general kinetic model for quantitative perfusion imaging with arterial spin labeling. *Magn Reson Med*. 1998, 40:383-96. [10.1002/mrm.1910400308](#)
10. Arnoldner MA, Gruber M, Syré S, Kristen KH, Trnka HJ, Kainberger F, Bodner G: Imaging of posterior tibial tendon dysfunction--comparison of high-resolution ultrasound and 3T MRI. *Eur J Radiol*. 2015, 84:1777-81. [10.1016/j.ejrad.2015.05.021](#)
11. Jezzard P, Chappell MA, Okell TW: Arterial spin labeling for the measurement of cerebral perfusion and angiography. *J Cereb Blood Flow Metab*. 2018, 38:603-26. [10.1177/0271678X17743240](#)
12. Takano N, Suzuki M, Irie R, et al.: Usefulness of non-contrast-enhanced MR angiography using a silent scan for follow-up after Y-configuration stent-assisted coil embolization for basilar tip aneurysms. *AJNR Am J Neuroradiol*. 2017, 38:577-81. [10.3174/ajnr.A5033](#)
13. Takano N, Suzuki M, Irie R, et al.: Non-contrast-enhanced silent scan MR angiography of intracranial anterior circulation aneurysms treated with a low-profile visualized intraluminal support device. *AJNR Am J Neuroradiol*. 2017, 38:1610-6. [10.3174/ajnr.A5223](#)
14. Hu HH, Pokorney AL, Stefani N, Chia JM, Miller JH: Non-gadolinium dynamic angiography of the neurovasculature using arterial spin labeling MRI: preliminary experience in children. *MAGMA*. 2017, 30:107-12. [10.1007/s10354-016-0589-5](#)
15. Oishi H, Fujii T, Suzuki M, et al.: Usefulness of silent MR angiography for intracranial aneurysms treated with a flow-diverter device. *AJNR Am J Neuroradiol*. 2019, 40:808-14. [10.3174/ajnr.A6047](#)
16. Katsuki M, Narita N, Ishida N, et al.: Usefulness of 3 Tesla ultrashort echo time magnetic resonance angiography (UTE-MRA, SILENT-MRA) for evaluation of the mother vessel after cerebral aneurysm clipping: case series of 19 patients. *Neurol Med Chir (Tokyo)*. 2021, 61:193-203. [10.2176/nmc.0a.2020-0336](#)
17. Kronthaler S, Diefenbach MN, Boehm C, et al.: On quantification errors of R2* and proton density fat fraction mapping in trabecularized bone marrow in the static dephasing regime. *Magn Reson Med*. 2022, 88:1126-39. [10.1002/mrm.29279](#)
18. Ljungberg E, Damestani NL, Wood TC, et al.: Silent zero TE MR neuroimaging: current state-of-the-art and future directions. *Prog Nucl Magn Reson Spectrosc*. 2021, 123:73-93. [10.1016/j.pnmrs.2021.03.002](#)
19. Bi X, Weale P, Schmitt P, Zuehlsdorff S, Jerecic R: Non-contrast-enhanced four-dimensional (4D) intracranial MR angiography: a feasibility study. *Magn Reson Med*. 2010, 63:835-41. [10.1002/mrm.22220](#)
20. Viswanath SE, Bloch NB, Chappelow JC, et al.: Central gland and peripheral zone prostate tumors have significantly different quantitative imaging signatures on 3 Tesla endorectal, in vivo T2-weighted MR imagery. *J Magn Reson Imaging*. 2012, 36:213-24. [10.1002/jmri.23618](#)
21. Azarine A, Garçon P, Stansal A, et al.: Four-dimensional flow MRI: principles and cardiovascular applications. *Radiographics*. 2019, 39:632-48. [10.1148/rg.2019180091](#)
22. Iryo Y, Hirai T, Nakamura M, et al.: Evaluation of intracranial vasculatures in healthy subjects with arterial-spin-labeling-based 4D-MR angiography at 3T. *Magn Reson Med Sci*. 2016, 15:335-9. [10.2463/mrms.tn.2015-0081](#)
23. van der Plas MC, Schmid S, Versluis MJ, Okell TW, van Osch MJ: Time-encoded golden angle radial arterial spin labeling: simultaneous acquisition of angiography and perfusion data. *NMR Biomed*. 2021, 34:e4519. [10.1002/nbm.4519](#)
24. Ding J, Duan Y, Wang M, et al.: Acceleration of brain susceptibility-weighted imaging with compressed sensitivity encoding: a prospective multicenter study. *AJNR Am J Neuroradiol*. 2022, 43:402-9. [10.3174/ajnr.A7441](#)
25. Ljungberg E, Wood TC, Solana AB, Williams SC, Barker GJ, Wiesinger F: Motion corrected silent ZTE neuroimaging. *Magn Reson Med*. 2022, 88:195-210. [10.1002/mrm.29201](#)
26. OsiriX DICOM Viewer. (2024). Accessed: 25th April 2024: <https://www.osirix-viewer.com/>.
27. Neural Network Console. (2024). Accessed: 25th April 2024: <https://dl.sony.com>.
28. Ronneberger O, Fischer P, Brox T: U-Net: convolutional networks for biomedical image segmentation. *Lecture Notes in Computer Science*. 2015, [10.1007/978-3-319-24574-4_28](#)
29. Physicochemical and pharmacokinetic profiles of gadopicleenol: a new macrocyclic gadolinium chelate with high T1 relaxivity: erratum. *Invest Radiol*. 2019, 54:810. [10.1097/RLI.0000000000000632](#)
30. Hochreiter S, Schmidhuber J: Long short-term memory. *Neural Comput*. 1997, 9:1735-80. [10.1162/neco.1997.9.8.1735](#)